Growth of thin Mn films on Si(111)-7×7 and Si(111)-$\sqrt{3}\times\sqrt{3}$:Bi

G. Ctistis,* U. Deffke, K. Schwinge, J. J. Paggel, and P. Fumagalli

Freie Universität Berlin, Institut für Experimentalphysik, 14195 Berlin, Germany

The growth process of Mn on two different reconstructions of the Si(111) surface is studied using reflection high-energy electron diffraction, low-energy electron diffraction with spot-profile analysis, scanning tunneling microscopy, and Auger-electron spectroscopy. Mn growth on both substrates—either by evaporation onto a substrate at room temperature with subsequent annealing or onto a substrate at elevated temperatures—leads to the formation of similarly structured epitaxial films with an extra layer of Si on top. Two growth models can be developed for the late stage of film growth on both substrates: Mn either grows in its γ phase or Mn forms MnSi. In contrast, differences are found in the beginning of the growth process, dependent on the underlying surface reconstruction.

INTRODUCTION

Mn is well known as a structurally complex element. Several structural phases are found in the temperature range between room temperature (RT) and 1250 °C: α-Mn (cubic, $a=8.89$ Å, stable up to $T=1070$ K),[1] β-Mn (cubic, $a=6.303$ Å, stable at $T>1000$ K),[2] γ-Mn (fcc, $a = [3.73$ Å (Ref. 3); 3.862 Å (Ref. 4)], stable between $T=1095$ and 1133 °C (Ref. 3) and δ-Mn [bcc, $a=2.715$ Å (Ref. 5) $a=3.0608$ Å, stable between $T=1133$ and 1244 °C (Ref. 4)]. α-Mn as the intrinsic RT phase contains 58 atoms per unit cell. At first, this does not seem to be a good basis for epitaxial growth but, on the other hand, such a complicated lattice may offer a large variety of possible slightly distorted lattices that can match a variety of substrates.

Up to now, only a few studies can be found in literature dealing with the growth of Mn on Si substrates. They mainly focus on very thin films of only the first few monolayers that grow epitaxially on the substrate.[6–11] Most of these publications indicate that Mn tends to form silicides when grown on a silicon substrate. Only two authors define their silicides in terms of lattice constant and stoichiometry: Lian and Chen observe tetragonal $MnSi_{1.7}$ with $a=5.531$ Å and $c=65.311$ Å,[8] whereas Zhang *et al.* find cubic MnSi with $a=4.557$ Å.[11] In this paper, we will compare the growth process of Mn [in a thickness range of up to 100 monolayers (ML)] on two different Si(111) surfaces: the native 7×7 and the Bi-induced $\sqrt{3}\times\sqrt{3}$ reconstruction.

EXPERIMENT

All experiments were performed in a standard oil-free three-chamber ultra-high vacuum (UHV) molecular-beam-epitaxy (MBE) system. The evolution of the crystalline structure during growth was monitored with reflection high-energy electron diffraction (RHEED). Low-energy electron diffraction with spot-profile analysis (SPA-LEED), Auger-electron spectroscopy (AES), and scanning tunneling microscopy (STM) measurements were performed in the analysis chamber. The pressure was below 10^{-9} mbar during Mn film growth and below 10^{-10} mbar during analysis. The samples are 12×12 mm^2 in size and mounted using tantalum clips on 2-in. molybdenum sample holders. Sample heating was accomplished by radiative heating of the entire Mo block from the back of the sample holder. Film thickness was monitored by a calibrated quartz microbalance mounted directly aside the sample growth position.

The preparation of the Si(111) surfaces includes the following steps: Si(111) wafers [both types, n-type doped (phosphorous) and p-type doped (boron)] are first treated chemically with an RCA-clean procedure[12] to obtain a clean protective oxide layer. This oxide is removed thermally under UHV conditions by heating the sample to 1200 °C for 2 min. A controlled cooling procedure leads to the formation of the Si(111)-7×7 surface reconstruction. Exposing the sample to a Bi flux equivalent to about 0.1–1.0 Å/min at 500 °C leads to a saturation coverage of 1 ML of Bi (as judged by AES) and forms a $\sqrt{3}\times\sqrt{3}$ reconstruction on the Si(111) surface.[13–15]

The Mn films were prepared by evaporation of Mn from a Knudsen cell with rates between 0.1 and 0.2 Å/min either at a substrate temperature of 250 °C [for growth on the Si(111)-$\sqrt{3}\times\sqrt{3}$:Bi surface] or 325 °C [for growth on the Si(111)-7×7 surface] or at RT with subsequent annealing to 250 °C. The Mn films had a nominal thickness of 2–100 ML, where 1 ML equals 7.83×10^{14} atoms/cm^2, the atom density of the Si(111) surface. The nominal thickness of 1 ML Mn as calculated from its α-phase structure is thus 0.952 Å.

RESULTS

Mn/Si(111)-$\sqrt{3}\times\sqrt{3}$:Bi

Certain aspects of the growth process on Si(111)-$\sqrt{3}\times\sqrt{3}$:Bi are discussed in Ref. 16. Here, we return to this topic for comparison and a better understanding.

When deposited at RT, Mn forms polycrystalline films. Post-growth annealing to 250 °C leads to well-ordered crystalline and flat structures as can be judged by electron diffraction and STM data (not shown here). In principle, the evolution of the film structure is comparable to what will be discussed for high-temperature growth below.
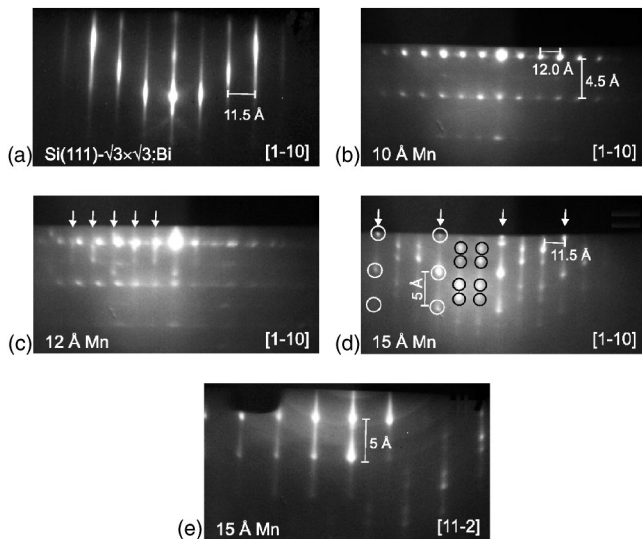
FIG. 1. RHEED patterns along the Si(111) $[1\bar{1}0]$ direction during growth of Mn on Si(111)-$\sqrt{3}\times\sqrt{3}$:Bi at 250 °C. (a) Substrate, (b) intermediate 3D Mn_5Si_3 phase, (c) transition to 2D phase, (d) 2D phase with characteristic point pattern, stable up to 120 Å Mn. (e) $[11\bar{2}]$-direction of 2D phase.

The series of RHEED patterns shown in Fig. 1 illustrates the main stages of the growth process at 250 °C: Starting with the $\sqrt{3}\times\sqrt{3}$ reconstructed surface (a), we first observe the formation of the first structural phase between about 4 and 13 Å deposited Mn film thickness. This phase is not only characterized by its three-dimensional-like diffraction pattern (spots, not on Laue circles) as shown in Fig. 1(b), but also exhibits an in-plane lattice constant being 5% larger than that one of the substrate. At ~12-Å nominal film thickness [Fig. 1(c)], a new structural phase (marked by the arrows) emerges. This structure is found to be stable from a nominal film thickness of 14 Å [Fig. 1(d)] to at least 120 Å. Figure 1(e) shows the RHEED pattern in the $[11\bar{2}]$ direction of the same thickness as Fig. 1(d). In contrast to the vanishing intermediate phase, the RHEED pattern now develops faint streaks as a sign of improving surface quality. The pattern is, however, still dominated by spots due to bulk diffraction. A characteristic spot structure is visible on the Bragg rods. The symmetry of this pattern is $\sqrt{3}\times\sqrt{3}$-like in the way that we find two types of spots: type one is marked by white circles and lies on the rods marked with arrows (corresponding to 1×1 rods). Type two, marked by black circles, is a double-spot structure on the two rods lying in between (corresponding to the $\sqrt{3}\times\sqrt{3}$ superstructure rods).

Although all these spots lie exactly on Bragg rods, they cannot be interpreted as simple high-surface-quality spots. To understand this, one has to remember the Ewald sphere as a model construction for reciprocal space. For high surface quality, one would expect only one spot on each lattice rod in the location where it is cut by the Ewald sphere. As a consequence, these spots should move along the rods (up and down) when azimuthally rotating the sample.[17] This is not observed. Furthermore, more than one intensity maximum is observed on each rod.

An interpretation as bulklike spots is also not straightforward as a comparison of the diffraction patterns of the two

high-symmetry directions $[1\bar{1}0]$ [Fig. 1(d)] and $[11\bar{2}]$ [Fig. 1(e)] demonstrates. In case of three-dimensional-like spots arising from periodicities perpendicular to the surface, we would find at least three different types of planes in Fig. 1(d): one corresponding to the spots on the 1×1-like rods and two belonging to the pairs of spots on the $\sqrt{3}\times\sqrt{3}$-like rods. These planes should be detectable in all directions, especially in $[11\bar{2}]$ [Fig. 1(e)]. But there, only the spots on the 1×1 rods are observed. We have to stress that in the transition region between clear transmission diffraction with spots and clear surface diffraction also with spots, transmission patterns from the selvage region are streaky. The RHEED patterns thus show features of surface diffraction as well as bulk diffraction, which is in good agreement with the surface morphology imaged by the STM.

The change from the spotty RHEED pattern in Fig. 1(b) to the pattern in Fig. 1(d) involves a remarkable phase transition: The first few layers grow in a relaxed nonpseudomorphic lattice structure. The lattice parameter is expanded by about 5% with respect to the substrate. At about 12 Å [Fig. 1(c)], a change back to the lattice parameter of the substrate is observed: The new pattern (arrows) has a slightly smaller lattice constant, as the increasing distance between streak and spots with separation from the center spot demonstrates. The RHEED pattern of Fig. 1(d) shows exactly the same lattice constant as the $\sqrt{3}\times\sqrt{3}$ reconstructed Si(111) surface. As already argued in Ref. 16, this can only be explained by the growth of two different structural phases, otherwise enormous strain energy would build up. For the start of growth, a pseudomorphic phase could be possible, which should then relax after a critical film thickness is reached. The reverse sequence is observed. Therefore the intermediate phase has to represent an equilibrium phase and cannot be substrate stabilized.

This is readily identified as the hexagonal Nowotny phase of Mn_5Si_3. In-plane and out-of-plane lattice constants match well to the respective parameters of 11.97 and 4.8 Å of hexagonal Mn_5Si_3.[16] This is not only consistent with the AES data to be discussed below, but also with recent photoelectron spectroscopy data by Kumar *et al.*,[18] where a Si bulk component and surface components in the Si 2p core level are detected. The identification of the film structure for thicker films is less simple. Before trying to solve this problem, we will first turn towards the growth of Mn films on the 7×7-reconstructed Si surface.

Mn/Si(111)-7×7

When deposited at RT, Mn again grows as a weakly polycrystalline film. Annealing the film to about 250 °C leads to flatter, albeit not perfect, crystalline structures manifested by a streaky RHEED pattern (not shown here). The structural features are comparable to what is shown in Fig. 2(c) for high-temperature growth.

Inspired by these observations and the studies by Evans *et al.*,[6] Mn was also deposited at a substrate temperature of 325 °C. Figure 2 shows the structural evolution during growth of 15 ML of Mn at this temperature. Right from the start, the 7×7 reconstruction disappears (a remnant of the
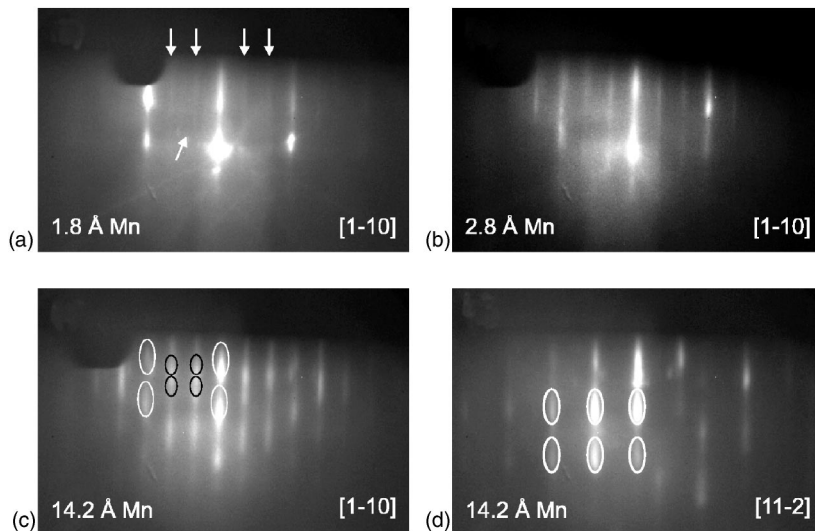
FIG. 2. RHEED patterns during growth of Mn on Si(111)-7×7 at 325 °C. (a)–(c) $[1\bar{1}0]$ direction from 2 to 15 ML, (d) $[11\bar{2}]$ direction at 15 ML, slightly distorted from the high-symmetry azimuth.

superstructure is marked by the single arrow). It is replaced by a Mn-induced $\sqrt{3}\times\sqrt{3}$ reconstruction. Two pairs of arrows mark the arising superstructure streaks in the $[1\bar{1}0]$ direction of the substrate at a thickness of 1.8 Å (a). Evans *et al.*[6] previously observed this superstructure. The $\sqrt{3}\times\sqrt{3}$ features become more intense with increasing Mn thickness [Fig. 2(b)], but the substrate Bragg rods from the Si lattice are still present. At 15 ML, the RHEED pattern reaches a stable configuration as shown in Fig. 2(c) for the $[1\bar{1}0]$ and Fig. 2(d) for the $[11\bar{2}]$ direction: The streaky pattern contains several intensity maxima on each streak. A careful investigation shows that these spots build the same characteristic pattern as the spots in Figs. 1(d) and 1(e) for the $[1\bar{1}0]$ and $[11\bar{2}]$ direction, respectively. This is marked by ellipses around the spots: white for features on the 1×1-like rods, black for the double-spot features on the superstructure rods. The two films are thus very likely of identical structure, but since the intensity maxima are comparatively broad, the surface quality is lower than that for growth on the $\sqrt{3}\times\sqrt{3}$ surface.

The distance between the streaks corresponds to a real-space distance of 11.5 Å, which exactly matches the lattice constant of the Si(111)-$\sqrt{3}\times\sqrt{3}$ reconstruction in this direction. The intensity distribution of the streaks in Fig. 2(c) is not that clear. Starting from the high-intensity specular rod in the center, a 1×1 symmetry is indicated by a continuously decreasing line intensity with increasing distance. This cannot be measured accurately because of the intensity modulations on each streak. These modulations even give the impression of high intensity for every other streak, suggesting a 2×2 symmetry. The pattern of the intensity maxima on the rods is, in principle, similar to the one shown in Fig. 1(d), as marked by the differently outlined ovals. The latter indeed has a $\sqrt{3}\times\sqrt{3}$-like symmetry. Therefore, from this measurement it is difficult to judge whether the symmetry of the observed pattern is still a $\sqrt{3}\times\sqrt{3}$ superstructure or has changed to a 1×1 structure or even a 2×2 superstructure. These three patterns produce an identical "spot distribution" in the RHEED and LEED experiments, just the intensity modulations are different—if one correspondingly assumes different base lattice constants. This will become clear in the

following discussion of the LEED patterns displayed in Fig. 3.

Figures 3(a) and 3(b) show diffraction patterns obtained from the 7×7 and the $\sqrt{3}\times\sqrt{3}$:Bi substrate reconstructions. The Si(111)-1×1 unit cell is marked by a solid diamond in subfigures (a)–(f). The diffraction pattern from the 15-ML Mn film on Si(111)-7×7 shown in Fig 3(c) indicates a $\sqrt{3}\times\sqrt{3}$ symmetry as judged from the intensity distribution of spots of different order: the spots located at positions expected for Si(111)-1×1 spots are more intense than the others. The overall intensity of the LEED patterns is relatively low, which is likely related to the small size of the crystallites forming the film on the scale of the coherence length of the electron beam used for the experiment (compare to STM results). Figure 3(d) shows the diffraction pattern of a 100-Å-thick Mn layer. At first glance, no obvious differences can be found between (c) and (d). Comparing the spot profiles as shown in the inset indicates that the quality of the sample does not deteriorate with increasing Mn thickness (at least in the range of 15–100 Å). The full width at half maximum (FWHM) in the spot profile is a direct measure for the underlying domain size of the crystallites.[19] It indicates domain sizes of ~40 Å for both samples 3(c) and 3(d). The momentum scale for the insets has a total length of 60% of the Si(111) Brillouin zone diameter.

Similar LEED measurements were performed for Mn films on the Bi-reconstructed surface. Figure 3(e) shows the LEED pattern for a 20-Å-thick Mn film, comparable to the one of Fig. 1(d). We find similar symmetry and FWHM as in Fig. 3(c), indicating a similar structure and surface quality. Differences can be found comparing the Mn films of 100-ML thickness [Figs. 3(d) and 3(f)]. In contrast to the film on the Si(111)-7×7 surface, we now observe an improvement of surface quality with increasing Mn thickness: the mean crystallite size becomes ~140 Å. In contrast to the unchanged k-space distribution of diffraction spots, for both pairs of patterns a more [3(e) and 3(f)] or less [3(c) and 3(d)] obvious change in spot-intensity distribution takes place. One major reason for spots to be brighter than others is that they arise from the underlying bulk structure. Thus, the most intense spots are very likely of 1×1 type, especially if this
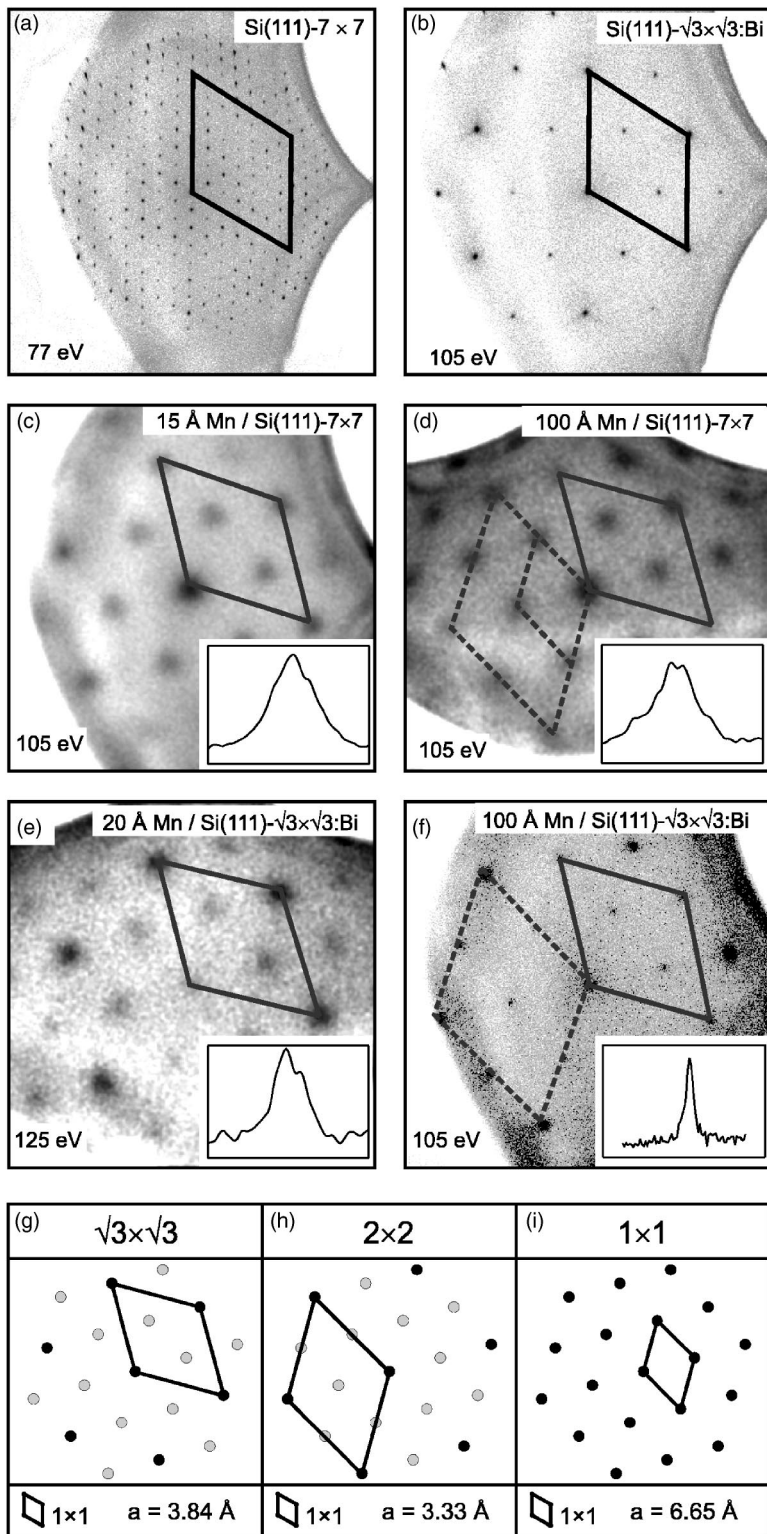
FIG. 3. (a) LEED pattern of the Si(111)-7×7 surface taken with 77 eV electrons. (b) LEED pattern of the Si(111)-$\sqrt{3} \times \sqrt{3}$:Bi surface reconstruction at 105 eV electron energy. The peak width in both images corresponds to about 1% of the Brillouin zone diameter. (c), (d): LEED patterns of $\sim$15 and 100 ML Mn grown on Si(111)-7×7 at 325 °C. (e), (f): LEED patterns of $\sim$15 and 100 ML Mn grown on Si(111)-$\sqrt{3} \times \sqrt{3}$:Bi at 250 °C. Possible reciprocal 1×1 unit cells are outlined. The solid diamonds indicate the Si(111) unit cell in k space. [Images (d) and (e) are rotated by 90° in order to obtain identical k-space orientation of the spots.] Each inset shows a distance of 60% of the Si(111) Brillouin zone with the smoothed profile of the most intense spots. (g)–(i) Schematic overview on the structural interpretation of the LEED images. Identical grids in k space with qualitatively different "intensity" ratios are displayed. 1×1-like spots are more intense (black circles), superstructure spots less intense (gray circles). Corresponding 1×1 lattice constants are indicated.

does not change with variation of the incoming electron energy.

As a consequence, different surface periodicities may produce identical k-space spot distributions, which differ in the spot-intensity distribution. With reference to the measured diffraction patterns, this is drawn schematically in Figs. 3(g)–3(i). Gray points display superstructure spots, black points represent high intensity and therefore 1×1-type spots.

The corresponding 1×1 unit cell is sketched, leading to the symmetry interpretation presented in each headline. The different 1×1 lattice constants are given at the bottom.

Following this discussion, both thinner films show patterns of $\sqrt{3} \times \sqrt{3}$ symmetry with a 1×1 unit cell as drawn in 3(c) and 3(e). The corresponding lattice constant is $a_{1 \times 1} = 3.84$ Å and therefore belongs to a Si(111) lattice. The intensity distribution of Fig. 3(f) then has to be interpreted as
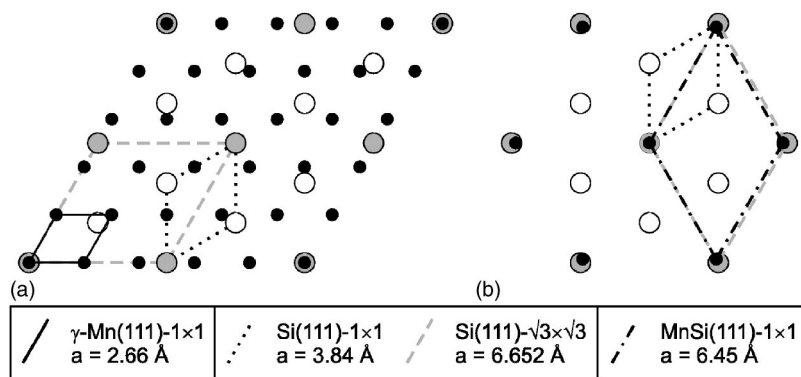
FIG. 4. Schematic of two possible growth modes of Mn on Si(111): (a) γ-Mn(111) on Si(111) with no lattice mismatch between $5 \times \gamma$-Mn(111) and $2 \times$ Si(111)-$\sqrt{3} \times \sqrt{3}$ (b) MnSi(111) on Si(111) with a lattice missmatch of 3% between MnSi(111) and Si(111)-$\sqrt{3} \times \sqrt{3}$.

a 2×2 reconstruction, although the spots have the same position in k space as in 3(e). Consequently, it is not a 2×2 reconstruction of the Si(111) lattice, but of a (111) lattice with a real-space lattice constant of $a_{1 \times 1} = 3.33$ Å, belonging to the marked 1×1 unit cell (dashed). This indeed, is no longer a Si(111) lattice constant but can serve as a sub lattice for Si(111)-$\sqrt{3} \times \sqrt{3}$. For the diffraction pattern of 100 Å Mn on Si(111)-7×7 [Fig. 3(d)], it is not unambiguous to find out which spots are of highest intensity. Therefore, an interpretation as 1×1, 2×2, or $\sqrt{3} \times \sqrt{3}$ superstructure is possible. The underlying 1×1 lattice constants of all these types of surface periodicities are indicated in Figs. 3(g)–3(i), respectively.

If we now compare the growth of Mn on both Si substrates by means of the diffraction experiments, two facts are most obvious: there is no intermediate Mn_5Si_3 phase for growth on the Si(111)-7×7 surface, and, for late stage growth, both films have similar structures exhibiting the Si lattice constant. This leads us back to the question, how to connect the Si lattice parameter at the film surface with the growth of well-closed epitaxial Mn films on a Si(111) substrate. Considering the different Mn phases listed in the beginning, two models can be developed for epitaxial growth just by structural arguments. Figure 4(a) shows that γ-Mn(111) can form a coincidence lattice with Si(111). The lattice constant of the hexagonal γ-Mn(111) surface is $a = 2.66$ Å. Thus, a 5×5-superstructure matches a 2×2 superstructure of Si(111)-$\sqrt{3} \times \sqrt{3}$. 13.30 Å = 13.304 Å is the identity for the lattice constants of γ-Mn(111)-5×5 and Si(111)-$\sqrt{12} \times \sqrt{12}$, respectively. A second model is based on the possiblity of further silicide formation as already mentioned by Zhang et al.[11] MnSi has a simple cubic structure with a lattice constant of 4.557 Å. The in-plane lattice constant of MnSi(111) is therefore $a = 6.45$ Å. This is only 3% smaller than the Si(111)-$\sqrt{3} \times \sqrt{3}$ lattice constant of $a = 6.652$ Å and leads to a good matching as demonstrated in Fig. 4(b).

Both models show that Mn can grow epitaxially on Si(111): either as γ-Mn(111) or as MnSi(111). Nevertheless, none of these models can directly explain the diffraction patterns shown before. The measured lattice constants simply are of Si(111)-$\sqrt{3} \times \sqrt{3}$ type and do not show any deviation from that. Thus they do not at all match γ-Mn. And, furthermore, they also do not match MnSi, since even a small deviation of 3% for MnSi as compared to the observed Si(111)-$\sqrt{3} \times \sqrt{3}$ should be detectable by RHEED.

AES and STM

To give more insight to what determines the surface structure, we present Auger-electron spectra of several Mn films grown on both substrates (Fig. 5). Spectra on the right side are taken from films deposited on the Si(111)-7×7 substrate, those on the left from films grown on the Bi-induced Si(111)-$\sqrt{3} \times \sqrt{3}$ reconstruction. Each series starts with a spectrum of the bare substrate at the bottom [5(a) and 5(b)], followed by spectra of the RT-grown film—15-ML Mn before [5(c) and 5(d)] and after annealing [5(e) and 5(f)] to 250 °C—and ends with the spectrum of the high-temperature grown film [20-ML Mn at 250 °C, Fig. 5(g); 15-ML Mn at 325 °C, Fig. 5(h)]. All spectra are scaled to identical maximum peak height to highlight the relative intensities in each spectrum.

Both RT spectra show a large amount of Mn (at 40 and 589 eV) and more Figs. 5(c) or less 5(d) intense peaks of the substrate materials Bi (101 eV) and Si (91 eV), respectively. While the Si signal in Fig. 5(d) might still originate from bare patches of the substrate, the comparison of Figs. 5(c) and 5(a) reveals that the detected Bi signal cannot originate from uncovered areas of the substrate. Otherwise, we should also detect a sizable amount of Si. Therefore, even at RT Bi is dissolved from the surface reconstruction and floats on top of the film, which is well closed as deduced from the small amount of Si in both cases. Bi behaves as surfactant[20] for the Mn growth. This may explain the better quality of the films grown on the Bi-reconstructed Si surface. Whether alloying takes place between Bi and Mn, either at RT or at higher temperatures, cannot be deduced from our data. If it does so, the alloy will to a large extent float on the surface of the film. In a forthcoming publication,[21] we will discuss the difficulties of growing MnBi in a controlled way on Si(111) substrates, which turned out to be impossible under the chosen conditions.

Annealing the RT-grown films restores a remarkable amount of Si in the Auger spectra [Figs. 5(e) and (f)]. Again, the first idea of interpretation is quite simple: the former well-closed films build crystalline islands and consequently large areas of the substrate become uncovered. The same could be stated for the high-temperature grown films [5(g) and 5(h)]. The STM images discussed below will, however, exclude this simple interpretation.

The STM images in Fig. 6 show 400×400-nm^2 large areas of nominally 100-Å- (a) and 35-Å- (b) thick Mn films grown on Si(111)-7×7 at RT with subsequent annealing at *nominally* 400 °C (a) and grown on Si(111)-$\sqrt{3} \times \sqrt{3}$:Bi at

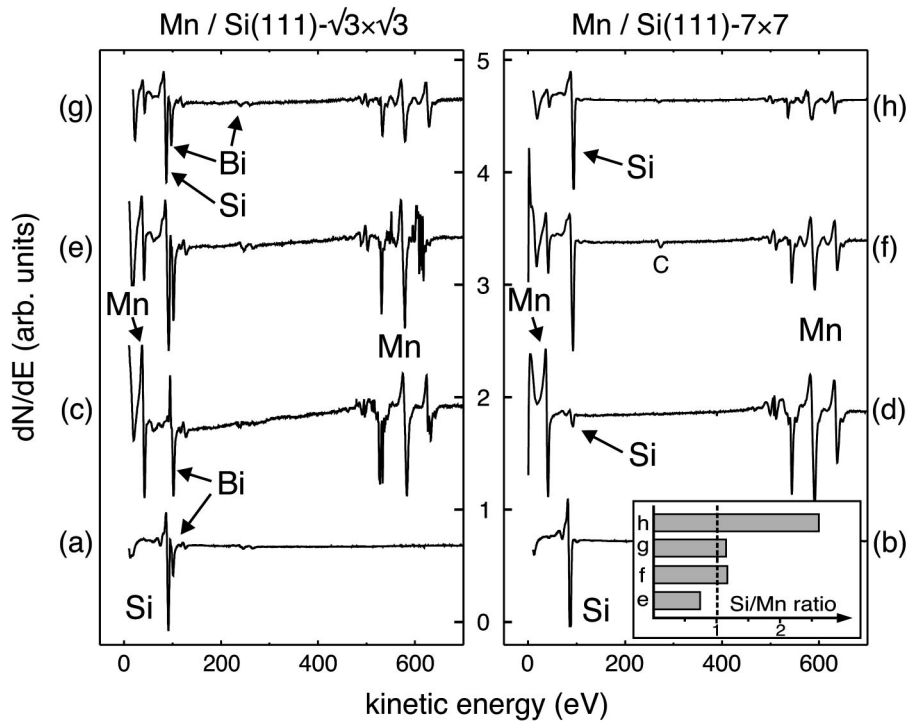FIG. 5. Two series of Auger spectra: Mn on Si(111)-7×7 (right) and on Si(111)-$\sqrt{3} \times \sqrt{3}$:Bi (left). Spectra of the bare substrate [(a), (b)], the RT-grown 15-ML films—before [(c), (d)] and after [(e), (f)] annealing to 250 °C, the high-temperature grown films [20 ML at 250 °C (g), 15 ML at 325 °C (h)]. The inset shows the Si_{91}/Mn_{589} ratios as calculated from the above spectra under consideration of sensitivity factors.

nominally 325 °C (b). The higher nominal temperatures for the STM samples are due to different sample holders used for STM measurements. (The STM samples have less contact with the sample holder, which requires higher *nominal* heater temperatures to achieve the same annealing effect on the sample as observed by RHEED.) We find a smoother surface with round-shaped densely packed atomically flat two-dimensional (2D) islands on the Bi-reconstructed surface, whereas on Si(111)-7×7 the flat islands are of triangular shape and the surface shows a slightly higher corrugation. The size of the flat terraces in (b) is approximately two or three times as large as in (a). This corresponds qualitatively to what was determined by SPA-LEED [Figs. 3(d) and (f)]. Nevertheless, a quantitative analysis shows striking differences between SPA-LEED and STM measurements. As stated before, the FWHM of the LEED spots of the high-temperature grown films belong to a domain size of around 40 Å on Si(111)-7×7 [Fig. 3(d)] and 150 Å on Si(111)-$\sqrt{3} \times \sqrt{3}$:Bi [Fig. 3(f)]. This is by a factor of 3 smaller as derived from the STM measurements and will be discussed in a forthcoming presentation.

The Mn films are well closed on the substrate. Only a few holes of ~7 nm [Fig. 6(a)] and ~5 nm [Fig. 6(b)] depth are found in both films (marked by circles). These holes may reach down to substrate regions but their diameter is not large enough to generate enough substrate signal to account neither for the large Si signal in AES nor for the diffraction data with Si(111) periodicity. The hole diameter is too small to reliably measure their bottom structure with STM. Instead, these holes may be the source for Si diffusing onto the surface and forming a Mn silicide. This leads us to the conclusion that the AES data give evidence for MnSi formation. No chemical shift can be detected neither in the Mn_{40} nor the Si_{91} peak position. The Si appears to be in a covalent bond just as under bulk Si conditions. All observations will be explained in a consistent picture if Si is assumed to dissolve from the substrate and to float on top of the film to form MnSi or a Si top layer during high-temperature growth or post-growth annealing. This phenomenon is observed for both substrates but shows slight differences in the reaction path as will be discussed in the following. A schematic representation of the proposed film structure is shown in Fig. 7.
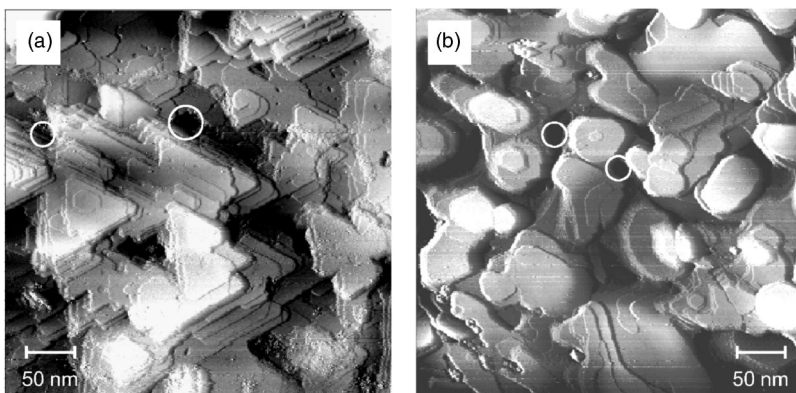

FIG. 6. STM pictures showing 400×400 nm² large areas of (a) a 100-Å Mn sample grown on Si(111)-7×7 at RT with subsequent annealing to nominally 400 °C and of (b) a 35-Å Mn sample grown on Si(111)-$\sqrt{3} \times \sqrt{3}$:Bi at nominally 325 °C substrate temperature.
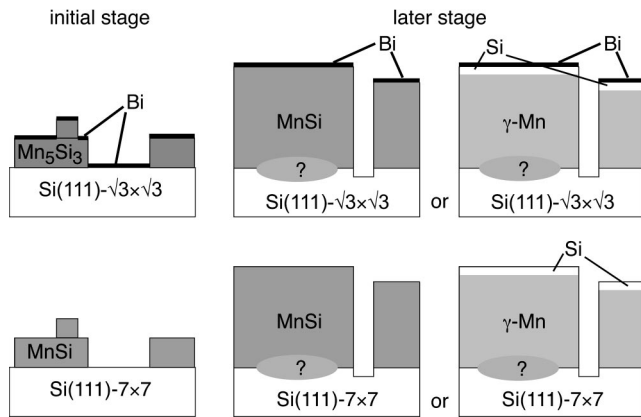
FIG. 7. Schematic representation of our model for the growth start (left) and later stages of film growth (right) for Mn films on Si(111)-$\sqrt{3} \times \sqrt{3}$:Bi (top row) and Si(111)-7×7 (bottom row) with the two alternative structures.

We up to now have no information on the buried interface between the film and the Si substrate. Maintaining Mn_5Si_3 at the interface would sandwich a material with a larger lattice parameter between the substrate and top layer with a smaller lattice parameter, rendering this configuration unlikely from the point of view of elastic energy in the film.

An analysis of the relative Auger peak intensities of Si and Mn gives an idea about the amount of Si in the topmost layer of the film. The peak-to-peak amplitudes for the Si_{91} and the Mn_{589} lines are divided by a sensitivity factor before further calculation according to Ref. 22. This procedure leads to the following ratios (Fig. 5, inset): (e) $Si_{91}/Mn_{589}=0.73$, (f) $Si_{91}/Mn_{589}=1.18$, (g) $Si_{91}/Mn_{589}=1.16$, (h) $Si_{91}/Mn_{589}=2.5$. Two trends can be identified: (i) Post-growth annealing leads to smaller amounts of Si than high-temperature growth even if a larger amount of Mn was deposited in the latter case [compare Fig. 5(g) to 5(e)]. (ii) Depositon on the pure Si substrate leads to larger amounts of Si than deposition on the Bi-reconstructed surface.

The first observation can be understood easily: If Si tends to diffuse to the top of the Mn film, this should be much easier during a growth process where the bare substrate areas offer a source of Si. Diffusion through the bulk of the RT-grown closed Mn films as necessary in the case of post-growth annealed films should be more difficult.

Except for the case of the post-growth annealed film on the Bi-covered substrate [Fig. 5(e)], the ratio Si_{91}/Mn_{589} is larger than 1. MnSi formation would lead to a ratio of $Si_{91}/Mn_{589}=1$. Therefore, an additional amount of Si is present on the surface. This is a very important statement for the interpretation of all our data because it helps to (at least partially) understand the Si-like diffraction patterns in terms of Mn growth. It also indicates that we indeed either observe a Si layer on top of the γ-Mn or a MnSi film. The growing film is able to exchange Si atoms with the substrate. The diffusion processes seem to be very efficient and allow the structures to stay close to thermal equilibrium.

Since the Auger data show Si on top of the films and the diffraction patterns point towards a Si lattice constant, a likely explanation is an excess Si layer on the film surface, which forms a silicon-induced reconstruction. The thickness of this film can be in the sub-ML regime (when the film is comprised of MnSi and then should be called Si-induced reconstruction), or 1–2 ML thick in the case of γ-Mn. The structure of Si and Mn phases match well and, consequently, one can grow epitaxially on the other no matter which species forms the surface and which the substrate.

On the Bi-reconstructed substrate, the upcoming Bi replaces part of that Si cover such that the Si/Mn ratio is lowered. Simply covering the film with Bi would not change the Mn/Si peak intensity ratio, as the attenuation due to the additional Bi film acts on both AES peaks the same way. If the film surface consists of a thin Si film on top of Mn, Bi would replace part of the film. If the film consists of MnSi, Bi replaces part of the Si in the selvedge region of the film. Subsurface Bi is unlikely due to electron counting: We are dealing with surfaces of three fold symmetry. A Bi adatom is thus likely to be located in a H3 adsorption site. Its five valence electrons then would saturate the bonds to the substrate and still fill the remaining dangling bond of a hypothetical sp^3-hybride orbital system. A subsurface Bi atom would have to be in a much more complicated environment.

In this article we cannot determine the nature of the bulk material. For sure, it has to be a Mn-containing phase. Core level photoemission data from the recent literature suggest the formation of a Mn silicide due to the presence of a surface component in the Si $2p$ spectra.[18] This would then rule out the γ-Mn possiblity; the experiment, however, ends at 5-ML Mn film thickness. Our identification as γ-Mn or MnSi has been derived just by structural argumentation, assuming crystallinity of the film and considering epitaxy conditions at the interface. No other evidence can be extracted from our data since they are based on surface-sensitive methods alone. We do not observe any changes in film characteristics for films thicker than ~15–20 ML. It should therefore be possible to extrapolate from the surface properties of the film to its bulk structure. The structure of the interface cannot be determined by our experimental methods.

SUMMARY

We investigated the growth of Mn on two different Si(111) surfaces: the 7×7 and the Bi-induced $\sqrt{3} \times \sqrt{3}$ reconstruction by means of electron diffraction (RHEED and SPA-LEED), Auger electron spectroscopy, and STM. Evaporation onto a substrate at RT yields polycrystalline structures. Subsequent annealing as well as evaporation at a substrate temperature of 250 or 325 °C leads to the growth of closed epitaxial films that are of similar structure on both substrates.

Since we have shown that either γ-Mn or MnSi can form a coincidence lattice with Si(111), we propose one of these Mn phases to build the bulk structure of the grown film. This has to be clarified in further experiments having access to the bulk region of the samples.

Although the growth leads to similar structures, the underlying growth process is different and shall be summarized in the following:

On the Si(111)-$\sqrt{3} \times \sqrt{3}$:Bi surface, the initial growth stage in the range of ~4 to ~12 Å leads to an island growth

of Mn_5Si_3. The lattice parameter as determined by RHEED and LEED matches the values from literature, and AES shows a large amount of Bi on top indicating its role as a surfactant. The thick film is similar to the one grown on the Si(111)-7×7 surface but of better surface quality compared to the thinner films and the ones grown onto the 7×7 surface. RHEED shows surface diffraction patterns intermixed with transmission patterns indicating a well-ordered, albeit not perfect surface. This is approved by STM images showing atomically flat islands. Their size of ~140 Å as determined by SPA-LEED is larger than that for the growth on the 7×7 surface, though by a factor 3 smaller than measured by STM. Auger data point toward a Bi- and Si-containing surface. The proposed structures, however, cannot explain the observed diffraction patterns since we observe a superposition of surface and bulk features.

On the Si(111)-7×7 surface reconstruction the growth starts with the formation of a Mn-induced $\sqrt{3} \times \sqrt{3}$ recon-struction on which MnSi or γ-Mn grows directly. The structure is of lesser quality, the island sizes are a factor 3 smaller than those for growth on the Bi-reconstructed surface, and the surface shows a slightly larger corrugation. This could explain the intensity differences as well as the higher background signal in the diffraction patterns. Again, Auger data point toward a Si-containing surface, as it detects an excess amount of Si on the surface. Since the diffraction data show no deviation from a Si(111)-$\sqrt{3} \times \sqrt{3}$ surface and cannot explain the proposed structures alone, further experiments are needed to clarify the bulk character of the thin films.

*Author to whom correspondence should be addressed. Email address: georgios.ctistis@physik.fu-berlin.de

[1] R. Wyckhoff, *Crystal Structures* (Wiley, New York, 1963).

[2] Konrad Sagel, in *Tabellen zur Röntgenstrukturanalyse*, edited by H. Mayer-Kaupp (Springer-Verlag, Berlin, 1958), Vol. VIII.

[3] D. Spisák, and J. Hafner, Phys. Rev. B **61**, 12 728 (2000).

[4] D. Tian, S. C. Wu, F. Jona, and P. M. Marcus, Solid State Commun. **70**, 199 (1989).

[5] S. Andriue, H. M. Fischer, M. Piecuch, A. Traverse, and J. Mimault, Phys. Rev. B **54**, 2822 (1996).

[6] M. M. R. Evans, J. C. Glueckstein, and J. Nogami, Phys. Rev. B **53**, 4000 (1996).

[7] S. Kawamoto, M. Kusaka, M. Hirai, and M. Iwami, Surf. Sci. **242**, 331 (1991).

[8] Y. C. Lian and L. J. Chen, Appl. Phys. Lett. **48**, 359 (1986).

[9] T. Nagao, S. Ohuchi, Y. Matsuoka, and S. Hasegawa, Surf. Sci. **419**, 134 (1999).

[10] S. M. Shivaprasad, C. Anandan, S. G. Azatyan, Y. L. Gavriljuk, and V. G. Lifshits, Surf. Sci. **382**, 258 (1997).

[11] Q. Zhang, M. Tanaka, M. Takeguchi, and K. Furuya, Surf. Sci. **507-510**, 453 (2002).

[12] W. Kern, *Handbook of Semiconductor Wafer Cleaning Technology* (Noyes, Norwich, NY, 1993).

[13] K. J. Wan, T. Guo, W. K. Ford, and J. C. Hermanson, Phys. Rev. B **44**, 3471 (1991).

[14] R. Shioda and A. Kawazu, A. A. Baski, C. F. Quate, and J. Nogami, Phys. Rev. B **48**, 4895 (1993).

[15] S. Nakatani and T. Takahashi, Y. Kuwahara, and M. Aono, Phys. Rev. B **52**, R8711 (1995).

[16] G. Ctistis, U. Deffke, J. J. Paggel, and P. Fumagalli, J. Magn. Magn. Mater. **240**, 420 (2002).

[17] A. S. Arrott, in *Ultrathin Magnetic Structures I*, edited by J. A.C. Bland and B. Heinrich (Springer-Verlag, Berlin, 1994).

[18] A. Kumar, M. Tallarida, M. Hansmann, U. Starke, and K. Horn, J. Phys. D **37**, 1083 (2004).

[19] M. Henzler, Appl. Surf. Sci. **11/12**, 450 (1982).

[20] M. Copel, M. C. Reuter, Efthimios Kaxiras, and R. M. Tromp, Phys. Rev. Lett. **63**, 632 (1989).

[21] U. Deffke, G. Ctistis, J. J. Paggel, and P. Fumagalli, J. Appl. Phys. **96**, 3972 (2004).

[22] L. E. Davis, N. C. MacDonald, P. W. Palmberg, G. E. Riach, and R. F. Weber, *Handbook of Auger Electron Spectroscopy*, 2nd ed. (Physical Electronics Industries, Edina, MN, 1976).